ADVANCED ENGINEERING MATERIALS
www.aem-journal.com

Influence of the Polymer Interphase Structure on the Interaction between Metal and Semicrystalline Thermoplastics

Liangyong Chu, Wouter J. B. Grouve, Martin van Drongelen, Yash Guha, Erik G. de Vries, Remko Akkerman, and Matthijn B. de Rooij**

It is demonstrated that a lamellar crystalline structure may form near the metal–polymer interface during the comolding of metal–thermoplastic joints. The influence of the crystalline morphology near the interface on the rupture behavior of the joint is studied experimentally. High-resolution scanning electron microscopy (HR–SEM), atomic force microscopy (AFM), and optical microscopy are used to characterize the microstructure of the metal–thermoplastic interface. The results show that a lamellar crystalline structure at the interface promotes cohesive failure, i.e., the crack runs in the polymer. Additional experiments show that a transcrystalline polymer structure at the interface results in failure at the interface. Herein, two methodologies have been developed to characterize the formation of the transcrystalline polymer interphase structure based on X-ray diffraction and polarized light hot stage microscopy. The results show the importance of the polymer interphase structure for metal–thermoplastic interactions. Understanding of the formation of the polymer interphase and its influence on the interfacial bonding strength are vital for thermoplastic applications such as fiber-reinforced thermoplastic composites, tool surface design for processing of thermoplastics, and their composites as well as for metal–polymer hybrid joints.

The metal–thermoplastic interaction is of significant importance since it i) determines the sticking of thermoplastics on the metallic mold surface and ii) dominates the bonding strength and long-term behavior of hybrid joints between metals and thermoplastics. Regarding the first aspect, sticking determines whether the thermoplastic parts can be successfully released from the metallic mold, e.g., after injection molding. In these cases, the bonding strength of the metal–thermoplastics interface needs to be minimized.[1] Regarding the second aspect, the bond strength between metals and thermoplastics is relevant in many applications, such as electronics, automotive, aircraft, adhesives, and polymer coatings.[2] The interaction between metals and thermoplastics is the key to maximize the bonding strength and its long-term behavior.[3]

Currently, metal–polymer interactions are understood in terms of physical adhesion and chemical bonding at the interface on different scales.[4] On the micrometer scale, mechanical interlocking is important, e.g., surface texturing has been used to improve metal–polymer adhesion.[5,6] On the smaller, molecular, or atomic scale, metal–polymer interaction is often explained in terms of physical attraction and chemical reactions between polymer chains and metal surfaces. Thus, various chemical treatments at the surface are used, e.g., plasma treatment or coupling agents have been applied to promote adhesion,[6,7] whereas silicone-based coatings are used to prevent adhesion.[8]

In this article, it is shown that the polymer interphase structure, the local polymer structure formed at the contact with the metal surface, strongly influences the rupture of the metal–thermoplastic interface. The polymer interphase at the contact with a metal surface is demonstrated to have a lamellar crystalline structure (crystal growth direction parallel to the metal surface). New weak points form in between the lamellar polymer interphase and bulk polymer, strongly affecting the rupture behavior of the metal–thermoplastic joints. Moreover, the alteration to a transcrystalline structure (crystal growth direction normal to the metal surface) in the polymer interphase causes a significant reduction of the bonding strength of the metal–thermoplastic joint. The role of polymer interphase is still a missing factor in the current understanding of metal–thermoplastic interactions. The results and methodologies in this article help the understanding of the formation of the polymer interphase, its role on the performance of the metal–thermoplastic bonding, and may guide the further tailoring of the interphase structures, which is crucial for both fundamental interfacial understanding and the practical application of thermoplastics.

First, the polymer microstructure in the bulk and at the metal–thermoplastic interface is characterized. **Figure 1**a shows the top view of a polyether ketone ketone (PEKK)–stainless steel specimen after melting and cooling. PEKK is highly crystallized

Dr. L. Chu, Dr. W. J. B. Grouve, Dr. M. van Drongelen, Y. Guha, E. G. de Vries, Prof. R. Akkerman, Prof. M. B. de Rooij
Department of Engineering Technology
University of Twente
7500 AE Enschede, The Netherlands
E-mail: l.chu@utwente.nl; m.b.derooij@utwente.nl

The ORCID identification number(s) for the author(s) of this article can be found under https://doi.org/10.1002/adem.202000518.

DOI: 10.1002/adem.202000518

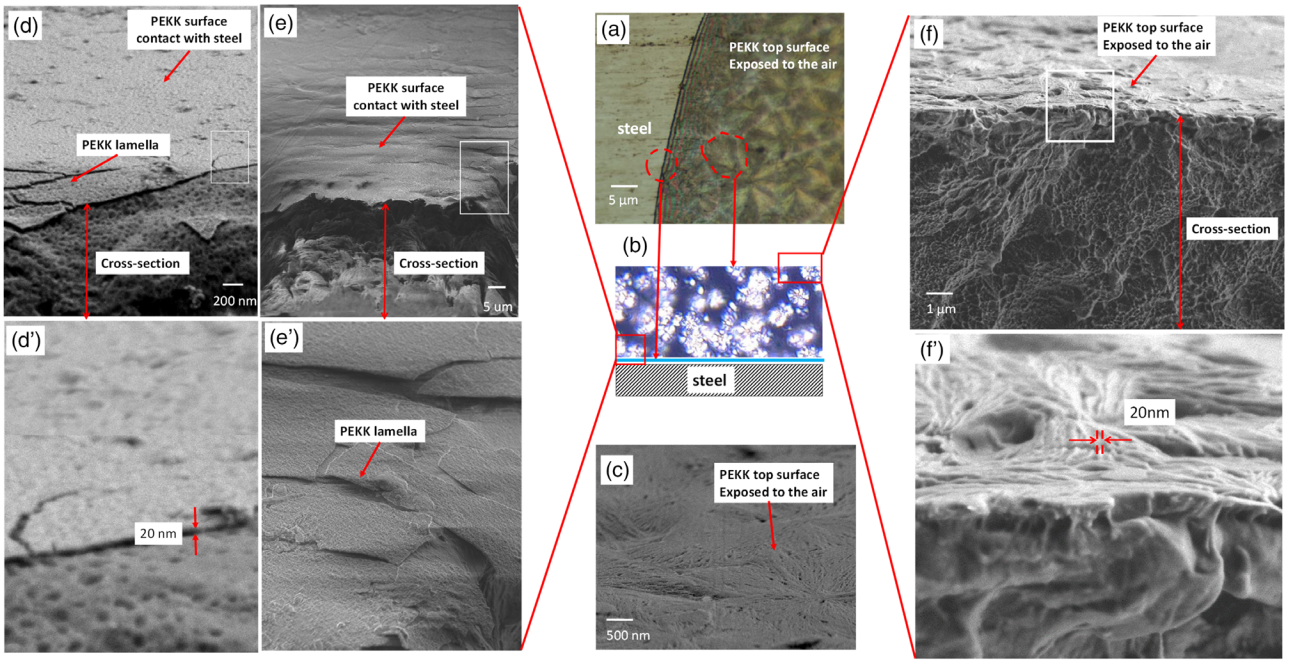

Figure 1. a) Top view of the PEKK–stainless steel specimen after melting and cooling using optical microscopy. b) Schematic drawing of the structure of the PEKK–stainless steel interface. c) HR–SEM image of the PEKK surface exposed to the air during sample preparation. d) HR–SEM image at the edge part of the cross section of the PEKK film after the steel substrate was chemically etched away. The cross section is prepared by bending and breaking the PEKK film in liquid nitrogen. d') HR–SEM image of the area in the white box of (d). e) HR–SEM image at the edge part of the cross section of the PEKK film after the steel substrate was chemically etched away. The cross section is prepared by bending and breaking the PEKK film at room temperature. e') HR–SEM image of the area in the white box of (e). f) HR–SEM image at the edge part of the cross section of the PEKK film near the surface exposed to the air during sample preparation. The cross section is prepared by bending and breaking the PEKK film in liquid nitrogen. f') High resolution scan of the area marked in white box of (f). The thickness of the PEKK lamellar crystal is ≈20 nm.

and spherulites are recognized in the bulk polymer as shown in Figure 1a. The spherulites are also recognized on the top surface, which was exposed to the air during sample preparation, as shown in Figure 1c and characterized using high-resolution scanning electron microscopy (HR–SEM). A layered structure is found in between the polymer spherulites and the steel surface. This region, of which structure is influenced by contact with the steel surface, is defined as polymer interphase. The steel substrate is chemically etched away to further characterize the structure of this polymer interphase. A cross section of the PEKK film was subsequently prepared, and HR–SEM was used to characterize the microstructure at the edge of the cross section. Figure 1d shows the morphology of the cross section of the polymer film prepared by bending and breaking the PEKK film at −70 °C (see experimental part). A layer structure with a thickness of ≈20 nm is recognized on the surface which was in contact with the metal. This layer is not found on the surface that was exposed to air during the sample preparation as shown in Figure 1c. Thus, this layered interphase structure is formed due to the contact with the steel surface. To further confirm the presence of this layered interphase structure, another PEKK polymer film is prepared using the same method as a repeated experiment. In this article, different from the first experiment, the cross section was prepared by bending and breaking the PEKK film at room temperature. Figure 1e,e' show the morphology of the polymer cross section. Compared to the cross section prepared at low temperature, more deformation of the PEKK film is recognized on the top surface of the polymer film. A broken polymer layer is recognized on the polymer surface at the contact with the steel surface. The thickness of this uniform polymer layer is similar to the thickness of a PEKK lamellar crystal as shown in Figure 1f,f' and is consistent with the thickness of a polyaryletherketone polymer lamellar crystal reported in literature.[9] These results prove that a lamellar crystalline polymer interphase forms at the contact with metal surfaces. Next, the rupture behavior of the steel–PEKK interface was studied and the morphology of the failure surface was characterized.

Figure 2 shows the characterization results of the failure surface of the steel–PEKK interface with a lamellar polymer interphase. Details about the debonding test can be found in the Experimental Section. As shown in Figure 2a, polymer residuals are found on the steel surface after debonding. The PEKK residuals are surrounded by a uniform film structure on the steel surface. This indicates that the crack starts in between the lamellar crystal and bulk polymer and further propagates into the bulk polymer. The thickness of the residual polymer film is ≈20 nm as characterized using atomic force microscopy (AFM). This thickness is very similar to the layered polymer interphase structure as shown in Figure 1d–e. The layered structure is also recognized on the polymer counterpart after debonding as shown in Figure 2c. These results confirm that in case a lamellar

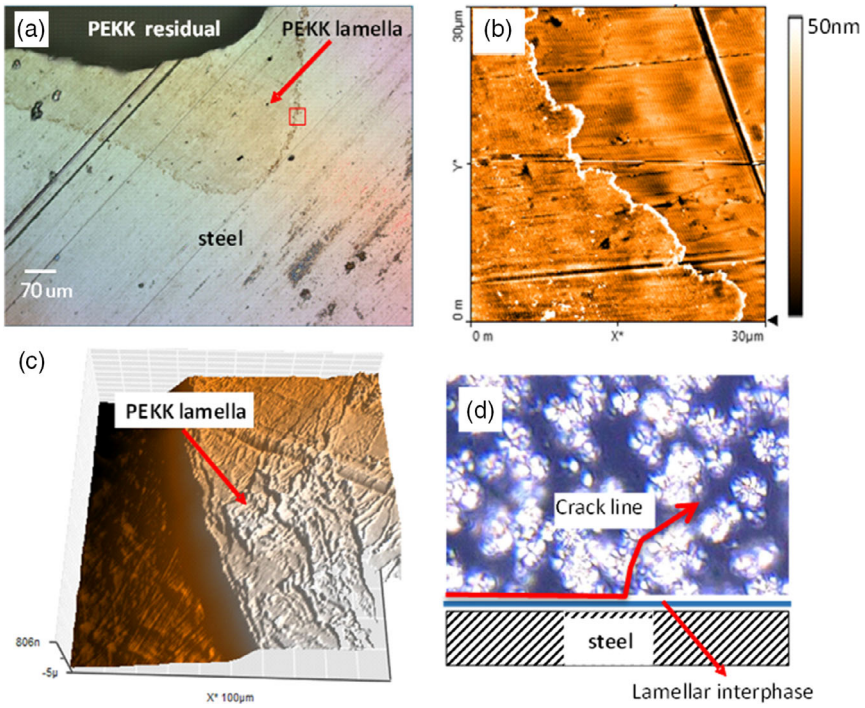

Figure 2. a) Optical image of the steel surface with PEKK residuals after debonding of the steel–PEKK joint. b) AFM height morphology of the red rectangular area in (a). c) AFM height morphology of the polymer counterpart after debonding. d) Schematic drawing of the fracture of the steel–PEKK joint with a lamellar crystalline interphase structure, the crack starts in between the lamellar crystal and bulk polymer and further propagates into the bulk polymer.

polymer interphase forms at the metal–thermoplastic contact, the crack starts at the polymer interphase and further propagates into the bulk polymer as schematically shown in Figure 2d. Since rupture is determined by the presence and location of weak points, the bonding strength between the lamellar crystal and metal surface seems larger than the bonding strength between lamellar crystal and bulk polymer. This can probably be explained by the larger Hamaker constant of the metal surface, which quantifies the van der Waals (VdWs) forces between two materials.[10] Possible chemical bonding between the polymer and metal surface can further enhance the bonding between the lamellar polymer interphase and the metal surface.[4] More debonding tests were performed using steel and various semicrystalline polymers samples including polyphenylene sulfide (PPS) and polyamide 6 (PA6), materials which are widely used in aerospace and automotive sectors.[11] After debonding, polymer residuals with a layered polymer structure are found for all these metal–thermoplastic interfaces (see Figure S1, Supporting Information). These results show that the formation of the polymer interphase structure, e.g., a lamellar crystalline structure, strongly influences the interaction between metal and thermoplastics.

According to the heterogeneous crystallization theory, the formation of the polymer interphase structure depends on surface chemistry, lattice matching, and surface energy.[12] For example, it has been reported that a transcrystalline structure forms when PEKK is in contact with a carbon fiber surface.[13] The growth of crystals normal to the fiber surface is caused by a high nucleation density of PEKK at the contact with carbon fiber surface. Using this information, a different polymer interphase is created to further study the influence of the polymer interphase structure on the metal–thermoplastic interaction. The polymer interphase is changed from lamellar to transcrystalline by using a graphene surface coating. Graphene is a 2D material composed of monolayer hexagonal sp^2 carbon atoms.[14] Two methodologies were used to characterize the structure of the polymer interphase at the contact with the graphene surface. First, hot stage microscopy using polarized light was utilized to study the formation of the polymer interphase structure at the contact with a graphene-coated surface (see Experimental Section and Figure S4, Supporting Information). A graphite flake made from mechanical exfoliation of highly oriented pyrolytic graphite (HOPG) was used to simulate a graphene-coated surface since it has the same chemical composition and lattice parameters as the graphene surface.[15] This thin graphite flake is folded and used in the polarized light hot stage microscopy experiments to create a graphite surface normal to the glass substrate. The graphite flake has a straight edge after it is folded as shown in **Figure 3**a. Figure 3a–c shows the PEKK polymer interphase formation at the contact with the folded graphite flake surface. The formation of a transcrystalline polymer interphase is recognized. As a comparison, the PEKK polymer interphase formation at the contact with a steel surface was also characterized as shown in Figure 3d–f. A steel fiber was used in these experiments. It is found that the polymer interphase structures formed at the contact with a graphene-coated surface and a steel surface

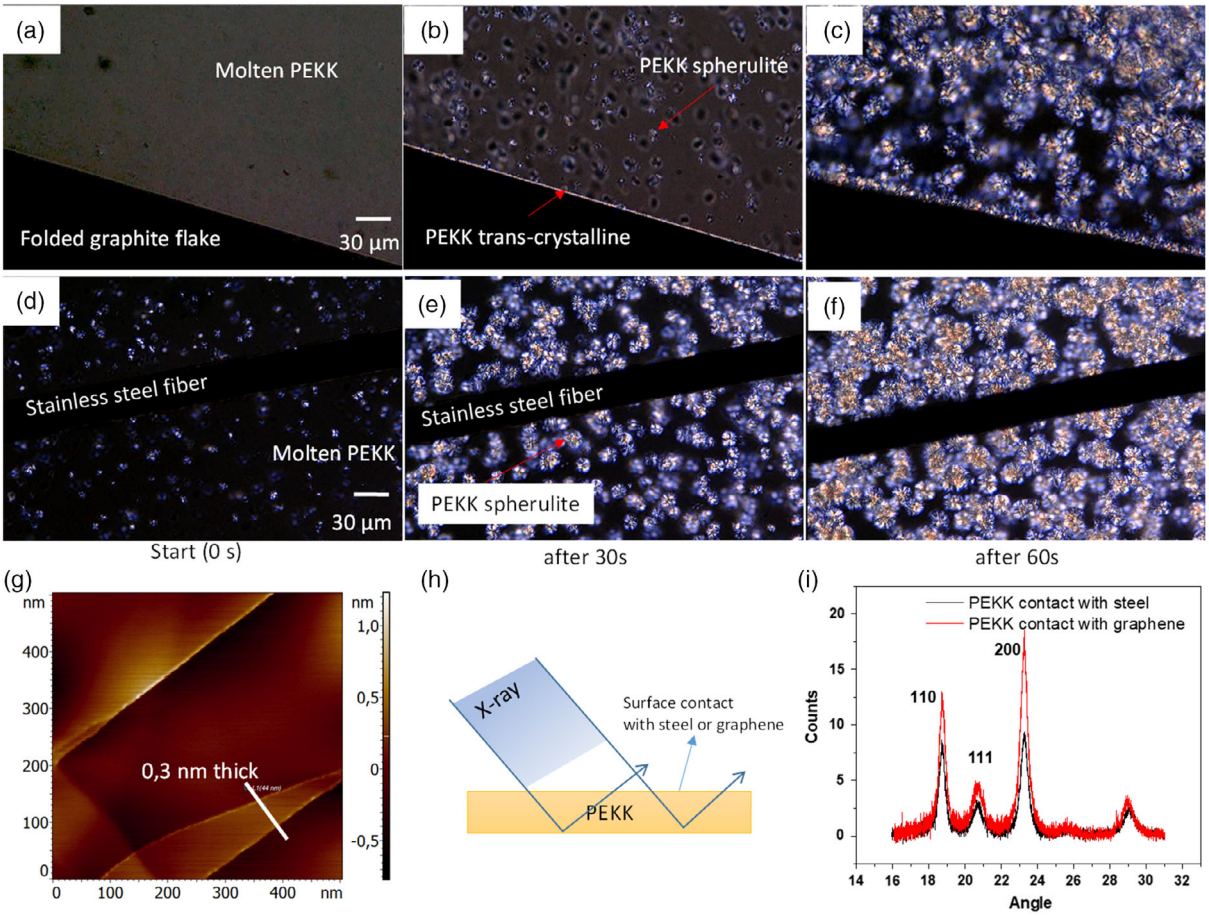

Figure 3. a–c) Molten PEKK polymer contact with graphite surface using the polarized light hot stage microscopy. The temperature of the isothermal crystallization of PEKK is 320 °C. A transcrystalline structure is recognized at the contact with the graphite surface. d–f) Polymer interphase structure at the contact with high-sticking stainless steel surface using the polarized light hot stage microscopy, no transcrystalline structure is found in the polymer interphase. The time interval between each image is 30 s, and magnification factor of all images is equal. g) AFM morphology of the graphite surface used in (a–c). Single-layer graphene with a thickness of ≈0.3 nm is found on the surface. h) Reflection mode XRD of the PEKK film contact with the high-sticking stainless steel surface and PEKK film contact with the nonsticking graphene-coated surface. i) XRD results of the PEKK at contact with the nonsticking surface and high-sticking surface. The intense peak corresponding to the (200) crystal plane corresponds to the formation of a transcrystalline structure.

are different. A transcrystalline polymer interphase is recognized at the contact with a graphene surface, whereas this was not found at the contact with a steel surface.

As the second methodology, X-ray diffraction (XRD) was used to further characterize the crystalline structure of the polymer interphase structure formed at the contact with a steel and a graphene-coated surface. Two PEKK films were melted and crystalized at the contact with a graphene-coated surface and a steel surface. Sample preparations for XRD characterizations can be found in the Experimental Section. Subsequently, these two PEKK films were characterized using XRD as shown in Figure 3h. The XRD patterns of the two PEKK films prepared at the contact with a graphene-coated surface and a steel surface are shown in Figure 3i. The XRD results show a two-chain orthorhombic cell of an edge-to-face phenyl packing lattice with dimensions of $a = 0.767$ nm, $b = 0.606$ nm, and $c = 1.008$ nm, which has been reported and well-accepted for the melt-crystallized PEKK.[16,17] The XRD peak at $2\theta = 23.3°$, which corresponds to the (200) plane of PEKK crystalized at the contact with the graphene-coated surface, increases 1.8 times compared to PEKK crystalized at the contact with a steel surface. The XRD analysis is shown in Figure S3, Supporting Information. An increasing number of the (200) planes that is parallel to the contact surface indicates the formation of the transcrystalline polymer structure at the contact with a graphene surface.[17] The polarized light hot stage experiments and the XRD characterizations confirm that a graphene coating can efficiently tune the polymer interphase structure to a transcrystalline structure.

Afterward, the bonding strength between the substrate and the thermoplastics with different polymer interphase structures was studied using a simple debonding test by opening a metal–thermoplastic joint. Experimental details about the debonding test can be found in the Experimental Section. **Figure 4**a shows the rupture surface of a steel–PEKK–steel joint. After debonding, PEKK residuals were found on the steel surface. The PEKK was strongly bonded to the steel surface such that the steel plate

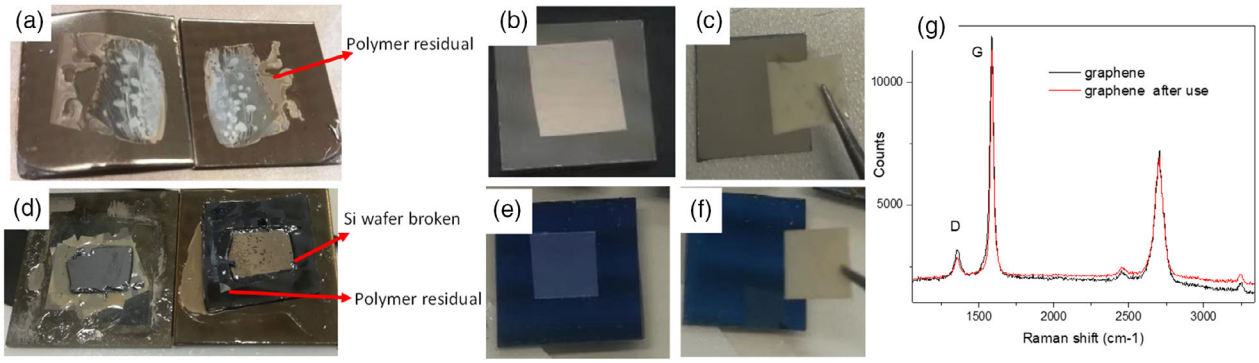

Figure 4. a) PEKK polymer residual on a high-sticking stainless steel surface after the debonding of stainless steel–PEKK film–stainless steel sandwich. b) PEKK film on graphene-coated nickel prior to melting. c) Peeling of the film using tweezers after melting and cooling. d) Debonding of the stainless steel–PEKK–silicon wafer (connected to a stainless steel plate) system. After debonding, the silicon wafer is broken and PEKK residuals are recognized on the Si surface. e) PEKK film on graphene-coated Si surface prior to melting. f) Peeling of the film after melting and cooling using tweezers. g) Raman spectrum of the graphene coating.

was plastically deformed during the debonding. Figure 4b,c show that the bonding strength of the metal–polymer joint is significantly reduced after the metal surface is coated with graphene. The PEKK film after melting and crystallization at the contact with graphene-coated nickel surface can be easily released from the substrate using a tweezer. This significant reduction of the interfacial bonding strength is also found for other thermoplastics including polyether ether ketone (PEEK), PPS, and PA6.

The significant reduction of the bonding strength of the metal–thermoplastic joints after the surface is coated with graphene cannot be readily explained based on current understandings about the metal–polymer interactions, e.g., a lower surface energy or decreased contact area. The surface energy of graphene is comparable to some high-sticking surfaces, e.g., glass,[18] and graphene can follow the surface roughness of the substrate due to its high flexibility. As a result, the adhesion between graphene and other materials is reported to be very strong.[19] Thus, this significant reduction of the bonding strength when the substrates are coated with graphene cannot be explained as a reduction of the surface energy or a reduction of VdWs forces. Furthermore, debonding tests have been performed using a single-crystalline Si wafer which is atomically flat. As shown in Figure 4d, the bonding strength of the Si wafer–PEKK joint is also strong. As a result, the silicon wafer was broken during the debonding of the joint. After the silicon wafer was coated with a single-layer graphene using a dry transfer method,[20,21] the bonding strength between PEKK and the silicon wafer was also significantly reduced. As shown in Figure 4e,f, the PEKK film after melting and crystallization at the contact with graphene-coated Si surface can also be easily released from the substrate using a tweezer. Thus, the significant reduction of the bonding strength when the substrates are coated with graphene cannot be explained as reduction of the surface roughness, which determines the real contact area. Another possibility is that graphene works as a boundary layer to reduce the adhesion,[8] thus, such that the graphene is transferred from the metal to the thermoplastic part. Figure 4g shows the Raman spectrum of the graphene-coated surface before and after being used for polymer fracture tests. As shown in Figure 4g, the D peak at 1350 cm^{-1} and G peak at 1583 cm^{-1} are recognized in the Raman spectrum of the graphene-coated surface. The D peak is caused by the disordered structure of the graphene and G peak corresponds to the stretching of the C—C bond in sp^2 carbon systems.[22] After using for easy releasing of PEKK, the ratio between D Peak and G peak remains the same, which shows that the graphene stays on the substrate and is not chemically oxidized or physically damaged.[22] It is consistent with the report that graphene is chemically stable in ambient conditions when the temperature is below 500 °C.[21,23] The Raman spectrum shows that the graphene coating is not transferred to the polymer part. Thus, the significant reduction of the bonding strength when the substrates are coated with graphene cannot be explained by the graphene working as a boundary layer.

Based on the fact that a transcrystalline polymer interphase forms when the interfacial adhesion is reduced, a hypothesis considering the polymer interphase structure is proposed to describe the underlying nonsticking mechanism. When a transcrystalline polymer interphase forms, the strength within the polymer interphase is much larger than that of the polymer–graphene interface. Meanwhile, the VdWs forces between graphene and metal are higher than the VdWs force between graphene and polymer, because of the high Hamaker constant of the metal.[10] As a result, during debonding, a crack is formed at the PEKK–graphene interface where the weakest point is located. These results show the potential of using graphene as an easy release coating that can be used in the processing of semicrystalline thermoplastics and their composites, as their processing (melting) temperature is much lower than the oxidation temperature of graphene, e.g., 375 °C for PEKK and PEEK.[24]

To conclude, the role of polymer interphase structure on semicrystalline polymer–metal interaction, which is not well understood so far, is studied in this article. A polymer interphase with a lamellar crystalline structure was found to form at the metal–thermoplastic interface. The presence of this lamellar crystalline polymer interphase strongly influences the rupture behavior, as it creates weak points within the polymer, between the interphase and the bulk polymer. More interestingly, it was demonstrated that the bonding strength of the

metal–thermoplastic interface can be significantly reduced by tuning the polymer interphase to a transcrystalline structure. This is probably because of the high bonding strength between the transcrystalline polymer interphase and bulk polymer. Our results on the polymer interphase structure formation and its influence on the interfacial bonding strength are vital for many engineering applications that involve interaction between metals and thermoplastic polymers, both from fundamental and practical aspects. These results and new methodologies may open up new subfield for thermoplastic polymer interface studies.

Experimental Section

Materials: The PEKK film was supplied by Cytec Industries. PEEK film was supplied by Victrex, UK. FORTRON 0214-PPS was supplied by Celanese company. PA6 was bought from Goodfellow, UK. AISI 430 stainless steel was supplied by Metaalketen, NL. Graphene-coated silicon wafer and graphene coated on nickel were purchased from Graphene Supermarket. HOPG was purchased from Sigma-Aldrich. Then, 4 mol L^{-1} H_2SO_4 solutions were prepared using 98.0 wt% sulfuric acid purchased from Sigma-Aldrich. A chip of about 1×1 cm^2 was cut from a (100) silicon wafer with a native oxide layer of about 2 nm obtained from Sil'Tronix Silicon Technologies.

Polymer Interphase Characterization: A Sensofar S Neox confocal microscopy was used for all the optical microscopy characterizations. A ZEISS MERLIN scanning electron microscope (SEM) was used to characterize the cross section of the PEKK film. All the SEM characterizations were operated at 1 kV. The magnifications shown in Figure 1c–f are 58 000, 228 000, 2000, and 11 500, respectively. To prepare the PEKK film used for SEM characterizations, a 1×1 cm^2 PEKK film with a thickness of 50 µm was placed on an AISI 430 stainless steel substrate. After melting at 375 °C for 5 min, the PEKK film at the contact with steel surface was cooled down and crystallized at the rate of 0.5 °C min^{-1}. Afterward, the stainless steel was chemically etched away using 250 mL H_2SO_4 solutions (4 mol L^{-1}). Two PEKK films crystallized at the contact with a steel surface were prepared using this method. To obtain information on the crystalline structure of the material cross section, the PEKK film was bended until it broke using two tweezers. The other PEKK film was put in liquid nitrogen for 10 min until there was no bubble formation on the polymer surface. The PEKK film was then bent until it broke using two tweezers in liquid nitrogen.

The surface of a piece of graphite flake mechanically exfoliated from the HOPG using a scotch tape was used to represent a graphene-coated surface. The surface morphology of the graphite flake was recognized using AFM. Monolayer graphene was recognized on the surface as shown in Figure 3g. The Raman spectrum showed that the graphite flake surface was composed of sp^2 carbon (Figure S2, Supporting Information). Thus, the graphite flake surface can well present a graphene-coated surface. The graphite flake was then folded and used in hot stage experiments. A THMS600 hot stage purchased from Linkam Scientific Instruments was used in conjunction with a Keyence polarized optical microscope. The schematic drawing of the setup can be found in Figure S4, Supporting Information. During the experiments, folded graphite flake–PEKK was put on the top of the transparent glass plate, afterward, the sample was heated up to 400 °C at a rate of 40 °C min^{-1}, after annealing for 5 min to remove all the PEKK crystals, the system was cooled down to 315 °C at a rate of 20 °C min^{-1}. PEKK was isothermally crystallized for 10 min at 315 °C. The same settings were used in the polarized light hot stage experiments of stainless steel fiber–PEKK system.

All samples that had been investigated using X-ray analyses were performed on a Bruker D8 Discover system equipped with a Cu tube. Wide-angle X-ray diffraction analyses were performed in reflection mode using a Lynxeye-XE-T detector in a scanning range of 16–31 degrees 2θ with a step size of 0.0035. A time per step of 0.5 s was used. Soller slits with an angle of 2.5 degrees were installed, a slide width of 0.6 mm was set on the primary side, and the detector opening was fixed to 2.05 mm. To prepare the sample for XRD characterization, two pieces of 10×10 mm^2 PEKK films with the same thickness of 50 µm were melted and cooled down at the contact with a steel surface and a graphene-coated nickel surface, respectively. The thermal treatment was the same for the two samples. The samples were melted to 375 °C at a rate of 20 °C min^{-1} and cooled down to room temperature at a rate of ≈0.5 °C min^{-1}. Afterward, the stainless steel of the high-sticking PEKK sample was chemically etched away using a 4 mol L^{-1} H_2SO_4 solutions. The nonsticking PEKK sample was released using a tweezer as shown in Figure 4c. To avoid the effect of chemical etching on the crystalline structure of the PEKK film, the easy releasing PEKK sample was also immersed in the H_2SO_4 solutions during chemical etching of steel–PEKK sample. The two PEKK samples were characterized using reflection mode XRD and the schematic drawing of the geometry is shown in Figure 3h. With this geometry, the strength of a certain XRD peak was proportional to the number of the corresponding crystalline plane with a direction that was parallel to the contact surface (the surface of the PEKK film).

Fracture Surface Characterization: For high-sticking surfaces such as steel and Si wafer surfaces, the sticking test was performed by placing a thermoplastic film in between two substrates. Afterward, the samples were melted and naturally cooled down to room temperature at a certain rate (≈0.5 °C min^{-1}) in an oven. The steel–PEKK–steel sandwich was mechanically separated. For a steel–PEKK–Si sandwich, because the silicon wafer was brittle, another stainless steel plate was fixed on the backside of the silicon wafer using glue (the front side of the silicon wafer sticked to the PEKK film). Afterward, the stainless steel–PEKK–silicon wafer (connected to a stainless steel plate) was mechanically separated. The silicon wafer broke during the debonding because of the strong adhesion force between the PEKK and the silicon surface.

A confocal Raman microscope (WITec Alpha300R, Germany) fitted with a UHTS300 spectrometer was used for the Raman measurements. The laser wavelength was 532 nm (WITec 532 nm laser). AFM morphology characterization was performed using a Park XE-100 AFM from Park Systems using an ACTA AFM probe purchased from AppNano. The spring constant of the probe was 26 N m^{-1} determined using the thermal noise method.[25]

Supporting Information

Supporting Information is available from the Wiley Online Library or from the author.

Acknowledgements

The authors acknowledge Dr. S. Wijskamp from ThermoPlastic composites Research Center (TPRC) and Dr. Yibo Su and Dr. M.R.S. Huisman from Brightlands Materials Center (BMC) for help with materials selection. The authors acknowledge Dr. M.A. Smithers from Mesa+ Institute for help with HR–SEM characterizations.

Conflict of Interest

The authors declare no conflict of interest.

Keywords

graphene, lamellar crystal, metal–thermoplastic interaction, polymer interphase, transcrystalline

Received: April 29, 2020
Revised: September 8, 2020
Published online:

[1] a) J. Wei, X. Zhu, L. Chen, J. Liu, C. Li, *Surf. Coat. Technol.* **2019**, *362*, 72; b) C. Urata, G. J. Dunderdale, M. W. England, A. Hozumi, *J. Mater. Chem. A* **2015**, *3*, 12626; c) P.-Y. Cheng, C. Lin, K.-Y. Tee, H.-Y. Lin, *Microsyst. Technol.* **2018**, *24*, 2823.

[2] a) G. G. Miller, D. M. Ivory, L. W. Shacklette, R. R. Chance, R. L. Elsenbaumer, R. H. Baughman, *Google Patents* **1983**; b) T. Clarke, K. Kanazawa, V. Lee, J. Rabolt, J. Reynolds, G. Street, *J. Polym. Sci.: Polym. Phys. Ed.* **1982**, *20*, 117; c) M. Zilberman, G. Titelman, A. Siegmann, Y. Haba, M. Narkis, D. Alperstein, *J. Appl. Polym. Sci.* **1997**, *66*, 243; d) R. Tao, X. Li, A. Yudhanto, M. Alfano, G. Lubineau, *Compos. Sci. Technol.* **2020**, *188*, 107964; e) R. Tao, M. Alfano, G. Lubineau, *Composites, Part A* **2019**, *116*, 216; f) J. Zhou, G. Lubineau, *ACS Appl. Mater. Interfaces* **2013**, *5*, 6189; g) X. Jin, J. Strueben, L. Heepe, A. Kovalev, Y. K. Mishra, R. Adelung, S. N. Gorb, A. Staubitz, *Adv. Mater.* **2012**, *24*, 5676.

[3] a) Y. Su, M. de Rooij, W. Grouve, L. Warnet, *Composites, Part B* **2016**, *95*, 293; b) M. Banea, L. F. da Silva, *J. Mater.: Des. Appl.* **2009**, *223*, 1; c) A. Kinloch, C. Korenberg, K. Tan, in *Durability of Structural Adhesive Joints*, Applied Sciences Publishers, New York **1983**; d) A. Puentes-Parodi, M. Gedan-Smolka, A. Leuteritz, M. Gehde, I. Kuehnert, *J. Compos. Mater.* **2018**, *52*, 3669; e) A. Heckert, C. Singer, M. F. Zaeh, R. Daub, T. Zeilinger, *Phys. Procedia* **2016**, *83*, 1083.

[4] Y. Su, M. de Rooij, W. Grouve, R. Akkerman, *Int. J. Adhes. Adhes.* **2017**, *72*, 98.

[5] a) K. Das, S. Bose, A. Bandyopadhyay, *Acta Biomater.* **2007**, *3*, 573; b) L. Monson, S. I. Moon, C. Extrand, *J. Appl. Polym. Sci.* **2013**, *127*, 1637; c) S. Hansson, M. Norton, *J. Biomech.* **1999**, *32*, 829; d) J. Byskov-Nielsen, J. V. Boll, A. H. Holm, R. Højsholt, P. Balling, *Int. J. Adhes. Adhes.* **2010**, *30*, 485.

[6] M. Akram, K. Jansen, L. Ernst, S. Bhowmik, *Int. J. Adhes. Adhes.* **2011**, *31*, 598.

[7] C. Ochoa-Putman, U. K. Vaidya, *Composites, Part A* **2011**, *42*, 906.

[8] G. W. Critchlow, R. E. Litchfield, I. Sutherland, D. B. Grandy, S. Wilson, *Int. J. Adhes. Adhes.* **2006**, *26*, 577.

[9] a) H. Wang, J. K. Keum, A. Hiltner, E. Baer, B. Freeman, A. Rozanski, A. Galeski, *Science* **2009**, *323*, 757; b) E. Baer, A. Hiltner, H. Keith, *Science* **1987**, *235*, 1015; c) D. A. Ivanov, B. Nysten, A. M. Jonas, *Polymer* **1999**, *40*, 5899; d) D. Ivanov, A. M. Jonas, *Macromolecules* **1998**, *31*, 4546.

[10] a) J. Lyklema, in *Fundamentals of Interface and Colloid Science: Soft Colloids*, Vol. *5*, Elsevier, Amsterdam/New York **2005**; b) L. Chu, A. V. Korobko, A. Cao, S. Sachdeva, Z. Liu, L. C. de Smet, E. J. Sudhölter, S. J. Picken, N. A. Besseling, *Adv. Mater. Interfaces* **2017**, *4*, 1600495.

[11] a) R. D. Farahani, M. Dubé, *Adv. Eng. Mater.* **2017**, *19*, 1700294; b) M. T. Byrne, Y. K. Gun'ko, *Adv. Mater.* **2010**, *22*, 1672; c) M. Akkapeddi, *Polym. Compos.* **2000**, *21*, 576.

[12] a) H. Schonhorn, *Macromolecules* **1968**, *1*, 145; b) A. Chatterjee, F. Price, S. Newman, *J. Polym. Sci.: Polym. Phys. Ed.* **1975**, *13*, 2369.

[13] E. J. Chen, B. S. Hsiao, *Polym. Eng. Sci.* **1992**, *32*, 280.

[14] a) A. K. Geim, *Science* **2009**, *324*, 1530; b) A. K. Geim, K. S. Novoselov, in *Nanoscience and Technology: A Collection of Reviews from Nature Journals*, World Scientific, Singapore **2010**, p. 11.

[15] K. S. Novoselov, A. K. Geim, S. Morozov, D. Jiang, M. I. Katsnelson, I. Grigorieva, S. Dubonos, A. A. Firsov, *Nature* **2005**, *438*, 197.

[16] C. Li, A. Strachan, *Polymer* **2019**, *174*, 25.

[17] K. H. Gardner, B. S. Hsiao, R. R. Matheson, B. A. Wood, *Polymer* **1992**, *33*, 2483.

[18] a) S. K. Rhee, *J. Mater. Sci.* **1977**, *12*, 823; b) S. Wang, Y. Zhang, N. Abidi, L. Cabrales, *Langmuir* **2009**, *25*, 11078; c) Y. J. Shin, Y. Wang, H. Huang, G. Kalon, A. T. S. Wee, Z. Shen, C. S. Bhatia, H. Yang, *Langmuir* **2010**, *26*, 3798; d) J. Rafiee, X. Mi, H. Gullapalli, A. V. Thomas, F. Yavari, Y. Shi, P. M. Ajayan, N. A. Koratkar, *Nat. Mater.* **2012**, *11*, 217.

[19] a) S. P. Koenig, N. G. Boddeti, M. L. Dunn, J. S. Bunch, *Nat. Nanotechnol.* **2011**, *6*, 543; b) S. Kumar, D. Parks, K. Kamrin, *ACS Nano* **2016**, *10*, 6552.

[20] a) D. Prasai, J. C. Tuberquia, R. R. Harl, G. K. Jennings, K. I. Bolotin, *ACS Nano* **2012**, *6*, 1102; b) X. Li, Y. Zhu, W. Cai, M. Borysiak, B. Han, D. Chen, R. D. Piner, L. Colombo, R. S. Ruoff, *Nano Lett.* **2009**, *9*, 4359; c) J. Kang, D. Shin, S. Bae, B. H. Hong, *Nanoscale* **2012**, *4*, 5527; d) D. Y. Wang, I. S. Huang, P. H. Ho, S. S. Li, Y. C. Yeh, D. W. Wang, W. L. Chen, Y. Y. Lee, Y. M. Chang, C. C. Chen, *Adv. Mater.* **2013**, *25*, 4521; e) K. S. Kim, Y. Zhao, H. Jang, S. Y. Lee, J. M. Kim, K. S. Kim, J.-H. Ahn, P. Kim, J.-Y. Choi, B. H. Hong, *Nature* **2009**, *457*, 706; f) L. Gong, I. A. Kinloch, R. J. Young, I. Riaz, R. Jalil, K. S. Novoselov, *Adv. Mater.* **2010**, *22*, 2694; g) S. Pang, Y. Hernandez, X. Feng, K. Müllen, *Adv. Mater.* **2011**, *23*, 2779.

[21] Y. Zhu, S. Murali, W. Cai, X. Li, J. W. Suk, J. R. Potts, R. S. Ruoff, *Adv. Mater.* **2010**, *22*, 3906.

[22] a) K. N. Kudin, B. Ozbas, H. C. Schniepp, R. K. Prud'Homme, I. A. Aksay, R. Car, *Nano Lett.* **2008**, *8*, 36; b) A. C. Ferrari, D. M. Basko, *Nat. Nanotechnol.* **2013**, *8*, 235.

[23] L. Xiaowei, R. Jean-Charles, Y. Suyuan, *Nucl. Eng. Des.* **2004**, *227*, 273.

[24] a) S. Z. Cheng, M. Cao, B. Wunderlich, *Macromolecules* **1986**, *19*, 1868; b) R.-M. Ho, S. Z. Cheng, B. S. Hsiao, K. H. Gardner, *Macromolecules* **1994**, *27*, 2136.

[25] a) H.-J. Butt, M. Jaschke, *Nanotechnology* **1995**, *6*, 1; b) L. Chu, M. Bus, A. V. Korobko, N. A. Besseling, *Ultramicroscopy* **2019**, *205*, 1.